

Anisotropy, damping, and coherence of magnetization dynamics in a 10 μm square $\text{Ni}_{81}\text{Fe}_{19}$ element

A. Barman, V. V. Kruglyak, and R. J. Hicken^{a)}

School of Physics, University of Exeter, Stocker Road, Exeter, EX4 4QL United Kingdom

A. Kundrotaite and M. Rahman

Department of Physics and Astronomy, University of Glasgow, Glasgow, G12 8QQ United Kingdom

(Received 2 January 2003; accepted 13 March 2003)

We have studied magnetization precession in a square $\text{Ni}_{81}\text{Fe}_{19}$ element, of 10 μm width, by time-resolved scanning Kerr effect microscopy. From the frequency of precession, we deduce a fourfold in-plane anisotropy of about 30 Oe at the center of the square. Larger damping of the precession was observed at the center of the element when the static field was applied parallel to a diagonal rather than to an edge of the square. Dynamic images show that the apparent increase in damping is associated with nonuniformity of the dynamic magnetization that is associated with the sample shape. © 2003 American Institute of Physics. [DOI: 10.1063/1.1572969]

Time-resolved scanning Kerr effect microscopy (TRSKEM) may be used to study precessional magnetization dynamics with unique spatiotemporal resolution.¹⁻³ Small magnetic elements are of interest for applications in magnetic recording technology, and magnetization dynamics have been studied in such elements by various techniques.¹⁻⁵ When a magnetic system is excited by a short magnetic field pulse, the evolution of the magnetization is determined by material parameters as well as the shape and size of the system, which control the interplay between exchange and dipolar interactions. TRSKEM allows various magnetic excitations within the system to be imaged. Substantial effort has been made to study magnetization reversal in continuous films and small elements.^{6,7} However, the coherence⁸ of precessional switching and the origin of the damping^{9,10} remain open questions. In this letter we present measurements of the precessional dynamics of a square $\text{Ni}_{81}\text{Fe}_{19}$ element. We use the variation of the precession frequency at the center of the square to characterize the in-plane magnetic anisotropy. Dynamic images will be presented that explain why the damping of the magnetization precession exhibits a strong dependence upon the orientation of the in-plane static field.

The sample was a square $\text{Ni}_{81}\text{Fe}_{19}$ element of 10 μm side and 150 nm thickness deposited on a glass cover slip substrate of thickness 0.17 mm and capped with a 20 nm protective layer of Al_2O_3 . The sample was prepared by electron beam lithography and sputtering. The sample preparation and the TRSKEM apparatus will be described in detail elsewhere.¹¹ An in-plane pulsed field with rise time of about 35 ps and peak amplitude of 27 Oe was applied to the sample by a transmission line connected to a photoconductive switch (Au on intrinsic GaAs).¹¹ Optical pump-probe measurements^{11,12} were performed at a wavelength of 790 nm. The sample was placed face down on the transmission line and the plane polarized probe beam was focused on the sample through the glass substrate by a cover slip corrected microscope objective (numerical aperture=0.65), so that

submicron spatial resolution was obtained. The pump beam was chopped and the polarization state of the backreflected probe beam was analyzed with an optical bridge detector and a lock-in amplifier. In the present study we have measured only the polar Kerr rotation of the reflected probe beam. The dynamic images were obtained by scanning the sample with respect to the fixed probe beam by means of a piezoelectric scanning stage. Two types of dynamic Kerr measurement were performed with the probe spot focused at the center of the element. First, the static field strength H was varied with the field vector \mathbf{H} parallel to the edge and diagonal of the element. Second, the orientation of \mathbf{H} (ϕ_H) within the plane of the sample was varied through 360° in steps of 10° while the value of H was kept constant. Figure 1 shows typical measurements of the time dependent Kerr rotation. The precession frequency was obtained from fast Fourier transforms, which showed a single mode in each case. In Fig. 2 the

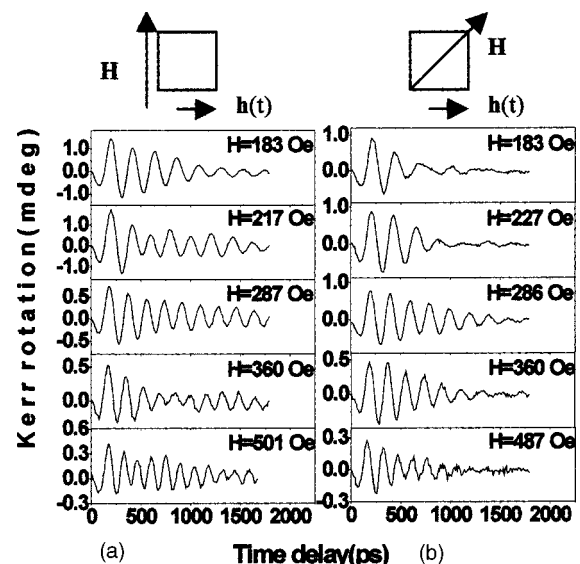


FIG. 1. Typical time dependent Kerr rotations at five different static field strengths for (a) $\mathbf{H} \parallel$ to an edge and (b) $\mathbf{H} \parallel$ to a diagonal are shown. The schematic at the top of the figure illustrates the relative orientations of the static (\mathbf{H}) and pulsed [$\mathbf{h}(t)$] field.

^{a)}Electronic mail: r.j.hicken@exeter.ac.uk

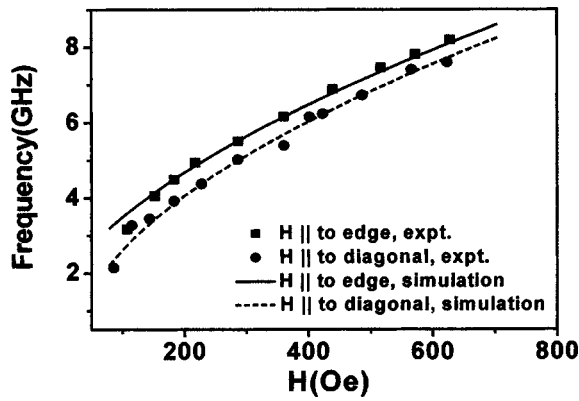


FIG. 2. Experimental precession frequencies (points) are plotted as a function of H for $\mathbf{H} \parallel$ to an edge and $\mathbf{H} \parallel$ to a diagonal. The simulated frequencies are shown as solid and dashed curves. The orientations of the static and pulsed field are as in Fig. 1.

extracted frequencies are plotted as a function of H for the two field orientations. In Fig. 3 the dependence of the frequency upon the orientation of \mathbf{H} is plotted for $H = 153$ Oe and $H = 410$ Oe. This reveals the presence of a fourfold symmetry with the maximum and minimum frequency occurring for \mathbf{H} parallel to the edge and diagonal, respectively.

The motion of the magnetization may be described by the Landau–Lifshitz equation.¹³ We assume that the energy density associated with the magnetic anisotropy has the form

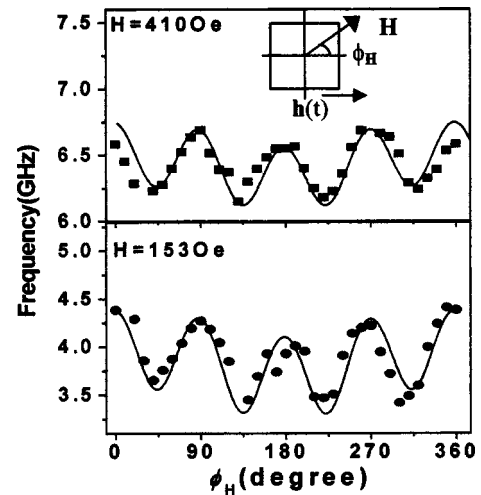


FIG. 3. Experimental precession frequencies (points) are plotted as a function of the orientation of \mathbf{H} for $H = 153$ Oe and $H = 410$ Oe. The simulated frequencies are shown as solid curves. The orientations of the static (\mathbf{H}) and pulsed [$\mathbf{h}(t)$] field are shown in the schematic at the inset of the figure.

$-K_2(\mathbf{u} \cdot \mathbf{k})^2 + K_4(u_x^4 + u_y^4)$ where K_2 and K_4 are the uniaxial and fourfold anisotropy constants, \mathbf{u} is a unit vector parallel to the magnetization vector, \mathbf{k} is a unit vector parallel to the uniaxial easy axis, and the x and y axes lie in the plane of the element parallel to its edges. The precession frequency is given by

$$f = \frac{\gamma}{2\pi} \left(\left[H \cos \phi + h \cos(\phi - \phi_h) + \frac{2K_2}{M} \cos 2(\phi - \phi_2) - \frac{4K_4}{M} \cos 4(\phi - \phi_4) \right] \times \left[H \cos \phi + h \cos(\phi - \phi_h) + \frac{2K_2}{M} \cos^2(\phi - \phi_2) - \frac{K_4}{M} [3 + \cos 4(\phi - \phi_4)] + 4\pi M \right] \right)^{1/2}, \quad (1)$$

where h is the magnitude of the time-averaged in-plane pulsed field, M is the magnetization, and ϕ , ϕ_h , ϕ_2 , and ϕ_4 are the angles made by the magnetization, the pulsed field, the uniaxial easy axis, and a fourfold easy axis with \mathbf{H} . The factor γ is equal to $g\mu_B/h$ where g is the gyromagnetic ratio.

The simulated frequencies in Figs. 2 and 3 were obtained with a single set of material parameters, and are in good agreement with the experimental frequencies. The uniaxial anisotropy field was found to be about 2 Oe in magnitude with the easy axis parallel to the edge along which a magnetic field of 150 Oe was applied during the sample deposition. The parameters used in the simulation of the frequencies were $4\pi M = 10.8$ kOe, $g = 2.1$, $4K_4/M = -33$ Oe, and $h = 12$ Oe. The presence of a fourfold symmetry in micron and nanometer sized square samples has been reported before for samples with different aspect ratios in a closely packed array.⁴ The demagnetizing field at the center of our element should be independent of the static field orientation if the element is uniformly magnetized. The fourfold anisotropy occurs because the element is not uniformly magnetized by the fields that we are able to apply.

The most striking feature of Fig. 1 is the larger damping of the oscillations when \mathbf{H} lies parallel to a diagonal rather

than to an edge. The pulsed field contains some secondary peaks due to reflections of the current pulse within the transmission line structure. These additional peaks can coherently enhance or suppress the motion depending upon their phase relative to the precession.^{14,15} This may cause the oscillatory Kerr signal to depart from a simple exponential decay as is sometimes observed in Fig. 1. However, the stronger damping that we observe for \mathbf{H} parallel to the diagonal is not the result of this coherent pumping mechanism. This is clear since the enhanced damping is observed for a range of different field values as the phase of the precession is varied relative to that of the secondary field peaks.

In order to further explore this observation, we have acquired a series of dynamic images with a field of 154 Oe applied parallel to the sample edge and diagonal. The delay between the pump and probe was fixed and the sample was scanned with respect to the fixed probe spot. The pixel size in each scan was $0.5 \mu\text{m} \times 0.5 \mu\text{m}$ and the gray scale in the images represents the out of plane component of the precessing magnetization. Figure 4 shows a few representative images from a series acquired at a large number of delay times. The pulsed field was parallel to the horizontal edge of the sample in all measurements. With \mathbf{H} parallel to the vertical

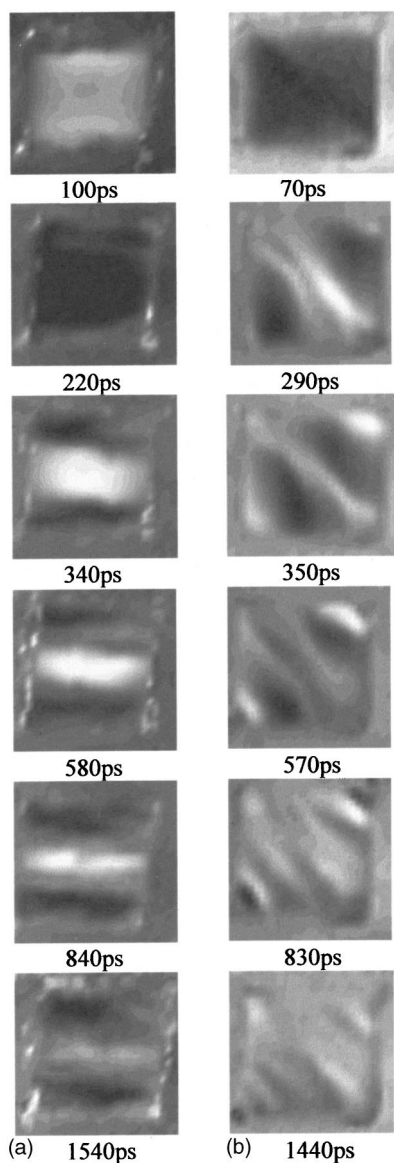


FIG. 4. Dynamic magnetic images are shown for a static field of 154 Oe applied (a) \parallel to an edge and (b) \parallel to a diagonal of the square. The times after excitation are shown at the bottom of each image. The orientations of the static and pulsed field are as in Fig. 1.

edge, nonuniformity first appears near the horizontal edges, and gradually moves towards the center of the element. The center of the element lies in the middle of a stripe that becomes narrower as time progresses, so that the magnetization is uniform over the area of the focused probe spot until long delay times. With \mathbf{H} parallel to the diagonal, a narrow stripe forms immediately at the center of the element. Again the stripe lies perpendicular to the static field. As time progresses, this stripe splits into two or more stripes so that the magnetization quickly becomes nonuniform across the area of the probe spot. The contrast at the center of the image is now reduced more quickly. The time resolved images strongly suggest that the apparent damping results from the excitation of long wavelength spin wave modes that super-

pose so as to reduce the average dynamic magnetization signal within the area of the probe spot. Micromagnetic simulations¹⁶ show that the nonuniform dynamic response begins from regions where the static internal field is nonuniform before the magnetic field pulse is applied. When \mathbf{H} lies parallel to the edge, regions of nonuniform internal field lie close to the edges that are perpendicular to \mathbf{H} . When \mathbf{H} is parallel to a diagonal, a region of nonuniform internal field is observed along the diagonal that lies perpendicular to \mathbf{H} . Consequently the nonuniformity of the dynamic magnetization spreads from different regions of the sample in the two cases.

In conclusion we have used TRSKEM to study the magnetization dynamics of a 10 μm square $\text{Ni}_{81}\text{Fe}_{19}$ element. Measurements of the time dependent Kerr rotation at the center of the element have revealed the presence of a four-fold anisotropy which we attribute to the internal field generated by the nonuniform static magnetization. The oscillatory Kerr signal appears more heavily damped when the static magnetic field is applied parallel to the diagonals of the square. The dynamic images have shown that this is associated with spatial nonuniformity at the center of the element. When \mathbf{H} is applied parallel to the edge of the element, the nonuniformity is confined to the edges until longer delay times. This work demonstrates that the shape of a thin film element can have a major influence upon the apparent damping of the magnetization precession.

The authors gratefully acknowledge the financial support of the UK Engineering and Physical Sciences Research Council.

- ¹W. K. Hiebert, A. Stankiewicz, and M. R. Freeman, *Phys. Rev. Lett.* **79**, 1134 (1997).
- ²Y. Acremann, C. H. Back, M. Buess, O. Portmann, A. Vaterlaus, D. Pescia, and H. Melchior, *Science* **290**, 492 (2000).
- ³J. P. Park, P. Eames, D. M. Engebretson, J. Berezovsky, and P. A. Crowell, *Phys. Rev. Lett.* **89**, 277201 (2002).
- ⁴S. M. Cherif, Y. Roussigne, C. Dugautier, and P. Moch, *J. Magn. Magn. Mater.* **242–245**, 591 (2002).
- ⁵M. M. Midzor, P. E. Wigen, D. Pelekhov, W. Chen, P. C. Hammel, and M. L. Roukes, *J. Appl. Phys.* **87**, 6493 (2000).
- ⁶W. K. Hiebert, G. E. Ballentine, and M. R. Freeman, *Phys. Rev. B* **65**, 140404 (2002).
- ⁷Th. Gerrits, H. A. M. van den Berg, J. Hohlfield, L. Bar, and Th. Rasing, *Nature (London)* **418**, 509 (2002).
- ⁸T. J. Silva, P. Kabos, and M. R. Pufall, *Appl. Phys. Lett.* **81**, 2205 (2002).
- ⁹J. Wu, N. D. Hughes, J. R. Moore, and R. J. Hicken, *J. Magn. Magn. Mater.* **241**, 96 (2002).
- ¹⁰M. Covington, T. M. Crawford, and G. J. Parker, *Phys. Rev. Lett.* **89**, 237202 (2002).
- ¹¹A. Barman, V. V. Kruglyak, R. J. Hicken, A. Kundrotaite, and M. Rahman (unpublished).
- ¹²R. J. Hicken and J. Wu, *J. Appl. Phys.* **85**, 4580 (1999).
- ¹³L. D. Landau and E. Lifshitz, *Phys. Z. Sowjetunion* **8**, 153 (1935).
- ¹⁴T. M. Crawford, P. Kabos, and T. J. Silva, *Appl. Phys. Lett.* **76**, 2113 (2000).
- ¹⁵M. Bauer, R. Lopusnik, J. Fassbender, and B. Hillebrands, *Appl. Phys. Lett.* **76**, 2758 (2000).
- ¹⁶A. Barman, V. V. Kruglyak, R. J. Hicken, A. Kundrotaite, J. Scott, and M. Rahman (unpublished).